To appear in: "Stellar Atmospheric Modeling",
Eds. I. Hubeny, D. Mihalas, K. Werner, Procs. Tübingen Conference,
Astron. Soc. Pac. Conf. Series,
Preprint: http://www.astro.uu.nl/∼rutten/

NLTE in a Hot Hydrogen Star: Auer & Mihalas Revisited

Jorrit Wiersma and Robert J. Rutten

Sterrekundig Instituut, Postbus 80 000, NL 3508 TA Utrecht, The Netherlands

Thierry Lanz

Goddard Space Flight Center, Code 681, Greenbelt MD 20771, USA

Abstract. We recompute the Auer & Mihalas (1969) hot-dwarf pure-hydrogen atmospheres for educational purposes, including comparison with full-atom modeling. Even the simple hydrogen model atoms employed by Auer & Mihalas provide rich radiative transfer complexity.

Introduction. This contribution is a tribute to two landmark papers published in the *Astrophysical Journal* by Auer and Mihalas in 1969. They modeled hot-dwarf ($T_{\rm eff} = 15\,000$ K, $\log g = 4$) hydrogen-only atmospheres, using two simplified hydrogen models:

- Auer & Mihalas (1969a): H I levels 1, 2 and c, Lyα (1-2) the only line;
- Auer & Mihalas (1969b): H I levels 1, 2, 3 and c, Baα (2-3) the only line.

They computed LTE-RE and NLTE-RE models for these atoms with the single line turned on and off. The resulting 2×4 models are shown in Fig. 1. In five subsequent "Non-Lte Model Atmospheres" ApJ papers they added more hydrogen levels and lines and other elements.

These seminal papers may be regarded as the practical start of NLTE stellar atmosphere modeling. Any student of stellar line formation should take them to heart – the more so because they remain highly instructive. They are "didactically correct" because, on the one hand, the simplicity of the two hydrogen models and the absence of other species enable easy identification of which spectral feature does what to the radiative-equilibrium atmosphere, while on the other hand the NLTE physics is already quite intricate – indeed extensively analysed by Auer & Mihalas in these papers. The two bare-atom models provide basic template examples for more complex situations in which richer model atoms may mix diverse population mechanisms to the level of unrecognizability.

The educational value of the Auer & Mihalas modeling is illustrated by the final exercise in Rutten's lecture notes[1] *"Radiative Transfer in Stellar Atmospheres"*. It asks the student to work through as many as four pages of questions concerning diagrams from the first paper alone! That exercise led to the present work, in which we recompute the Auer–Mihalas hot-hydrogen-star

[1] Available at URL `http://www.astro.uu.nl/∼rutten`

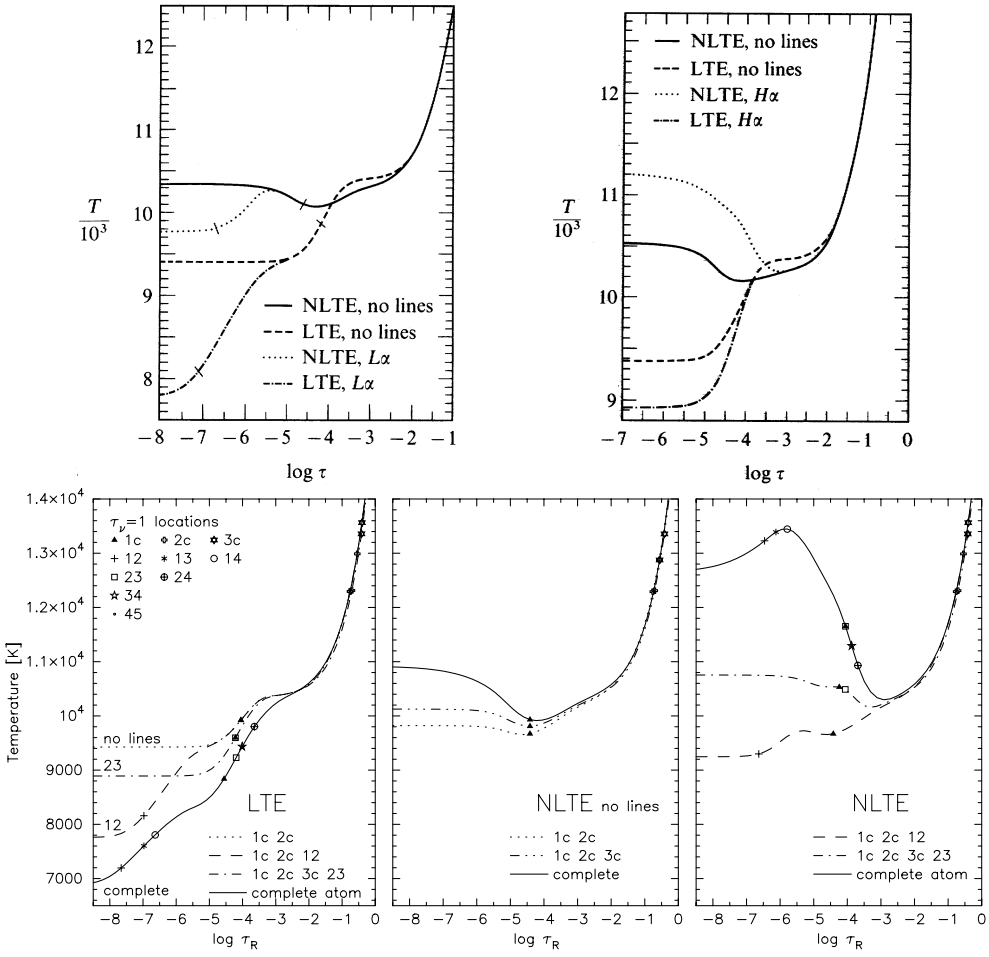

Figure 1. Upper panels: Auer-Mihalas models redrawn from Auer & Mihalas (1969a, b), copied from p. 434–435 in Mihalas' *"Stellar Atmospheres"* (1970; in the 1978 edition they appear on p. 215 and 242). The abscissae specify continuum optical depth τ at $\lambda = 400$ nm. Left: lowest two hydrogen levels plus continuum, LTE and NLTE, Lyα switched off and on. Right: lowest three levels plus continuum, LTE and NLTE, Baα switched off and on. The tick marks in the lefthand panel show $\tau_\nu = 1$ locations for the center of Lyα and the Lyman continuum. Lower panels: TLUSTY models, respectively LTE, NLTE without lines, NLTE with lines, for similar and for complete model atoms (see curve coding). The abscissae specify Rosseland optical depth $\tau_{\rm R}$. The symbols identify $\tau_\nu = 1$ locations for different spectral features as indicated in the first panel (at the line center and edge frequencies).

models with TLUSTY and add modeling with a complete hydrogen atom for comparison. Our motivation for this 33-years-later Auer–Mihalas re-visitation is twofold:

– to add diagnostic diagrams to the ones published by Auer & Mihalas, in particular B_ν, J_ν, S_ν graphs to illustrate the role of the radiation field and radiative heating & cooling graphs to illustrate the radiative energy budget. Such diagrams, given below, enrich the educational content of the Auer & Mihalas work even more. Their format was inspired by the well-designed displays in Vernazza et al. (1981)'s monumental paper, making our contribution also a tribute to Gene Avrett — another giant in our field attending this meeting[2].

– to display the effect of adding the rest of the hydrogen atom.

Auer & Mihalas models. The Auer–Mihalas models in the first panel of Fig. 1 show that the Balmer continuum, the Lyman continuum and the Lyα line reach their $\tau_\nu = 1$ escape depth at very different depths (1-2 and 1-c ticks; $\tau_{2c} = 1$ falls outside the plot). Each feature therefore leaves its own signature in the RE temperature structure. Easy to grasp are the three corresponding temperature drops due to LTE photon losses. The two-level-atom paradigm explains the diminished surface cooling by Lyα when NLTE-scattered. Less easy is that the Lyman continuum suffers similar resonance scattering ($\overline{S_{1c}} \approx \overline{J_{1c}}$ — are you sure that your code admits such bound-free scattering?)

More difficult are the slight outward temperature rise of the NLTE models ("Balmer continuum heating") and its substantial growth in the righthand plot when Baα is switched on. *"Amazingly, the photon losses in the subordinate Balmer-α line, located in the low-energy red part of the spectrum, cause heating of the whole outer atmosphere of this hot star."* Would you dare ask your students how this comes about?

TLUSTY models. We used TLUSTY (Hubeny & Lanz 1995) to compute twelve RE models for the Auer-Mihalas pure-hydrogen atmosphere:

LTE 1c, 2c	LTE 1c, 2c, 3c	LTE complete, no lines
NLTE 1c, 2c	NLTE 1c, 2c, 3c	NLTE complete, no lines
LTE 1c, 2c, 12	LTE 1c, 2c, 3c, 23	LTE complete, all lines
NLTE 1c, 2c, 12	NLTE 1c, 2c, 3c, 23	NLTE complete, all lines

The column 1 models correspond to Auer & Mihalas (1969a), the column 2 models to Auer & Mihalas (1969b), the column 3 models to the state of the art: 16 explicit-NLTE levels, 1 NLTE super-level which groups levels 17–80, Rydberg level dissolution using the Hummer formalism, the Lyman, Balmer, Paschen and Brackett lines computed with Stark profiles, level 5–10 lines computed with Doppler profiles, and lines with $n > 10$ lines put in radiative balance. Note that CRD is still assumed for all transitions, even Lyα. We produced diagnostic graphs for all 12 models but can only show a few here.

The lower panels in Fig. 1 show the resulting temperature stratifications for ten of these models. The Auer-Mihalas-like models agree well enough with the original Auer–Mihalas results, given slight differences in bound-free edge profile sampling, line shapes, and high-level treatment.

---

[2] ADS shows that Avrett published already in 1961, Mihalas in 1962, Auer in 1964.

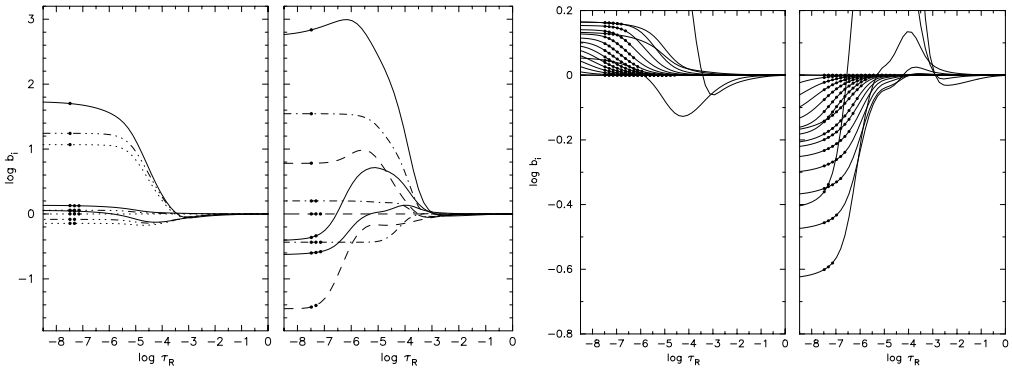

Figure 2. Population departure coefficients $b \equiv n/n^{\rm LTE}$ for models without lines (panels 1 and 3) and for models with lines (panels 2 and 4). Level numbers are specified by dots. First pair: low levels, different models curve-coded as in the 2nd and 3rd temperature stratification plots in Fig. 1. Second pair: more levels, complete hydrogen model.

The complete NLTE model has a yet higher outward temperature rise because its "ladder" of Rydberg levels permits a diffusive population flow from the ion population reservoir down to $n = 3$.

NLTE population departures. Figure 2 shows population departure coefficients, for low levels in different model without and with lines and for high levels in the complete models without and with lines. The $n = 1$ ground state gathers large NLTE overpopulation drawn down from the $b \approx 1$ ion reservoir by photon losses in Baα, enhancedly when the Rydberg ladder is in place (second panel). The latter is evident in the righthand panels. Its sequential $b_{i+1} \neq b_i$ steps transport population collisionally upwards or downwards to or from the ion reservoir depending on the lower-level boundary constraints. The $b_{i+1} > b_i$ departure divergence at right results from Baα photon suction (Bruls et al. 1992) and produces emission lines from Brackett α (45) longward (Auer & Mihalas 1969c): a collisionally-governed NLTE emission mechanism! In the solar spectrum such Rydberg emission is initially dominated by identical but more abundant Rydberg levels of Mg I, causing the well-known Mg I 12-micron emission lines (Carlsson et al. 1992); solar hydrogen emission lines appear at longer wavelengths (Carlsson & Rutten 1992). See Rutten & Carlsson (1994) for explanation.

Note that the Lyman $\tau_{\rm R} = 1$ locations move slightly inward from LTE to NLTE in Fig. 1. The ground state overpopulation is compensated by increased ionization from the higher NLTE temperature. Population density plots (not shown) as those in Auer & Mihalas illustrate that the concentrations and $\tau = 1$ locations vary less than the temperature structure: radiation losses are more important than temperature in controlling populations.

S, B, J graphs. Figure 3 diagnoses the formation of the Lyman, Balmer and Paschen continua from the complete-atom NLTE model in the graphical format

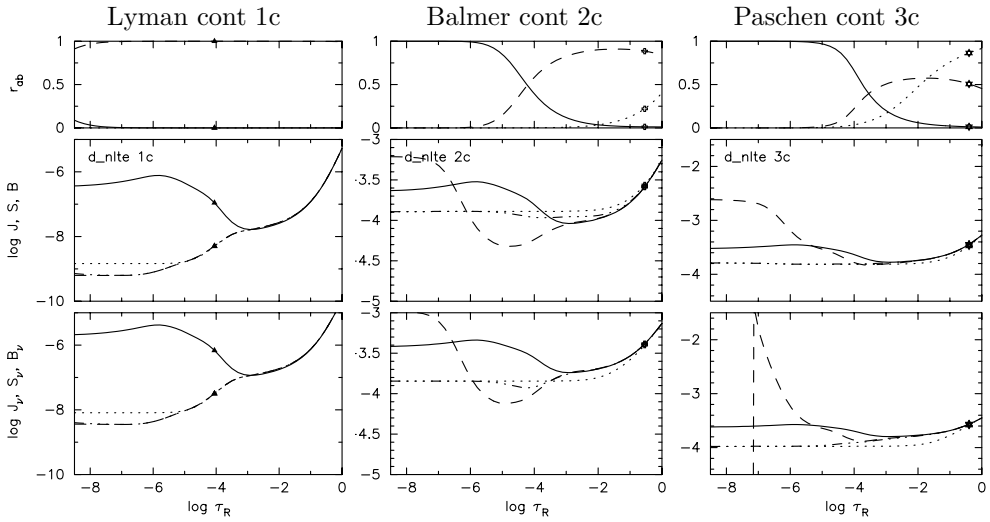

Figure 3. Avrett-style continuum formation diagrams for the three principal hydrogen edges. Top panels: relative contributions to the extinction by the pertinent edge (dashed) and by Thomson scattering (solid). Dotted: collisional transition fraction. Marks: $\tau = 1$ depths at threshold. Middle and bottom panels: total source function (dash-dotted), transition source function (dashed), Planck function (solid), mean intensity (dotted). Middle panels: averaged over the whole edge. Bottom panels: monofrequent, at threshold.

developed by Vernazza et al. (1976) and used to produce Fig. 36 of Vernazza et al. (1981), probably the most informative display in stellar atmosphere physics[3].

Note the multi-level departures from two-level behavior (requiring S to lie between J and B according to $S = (1 - \varepsilon)\, J + \varepsilon B$) in all three continua, the dominance of resonance scattering ($S \approx J$) in the Lyman continuum up to $\log \tau_{\rm R} \approx -5$), the negative flux divergence $\overline{J} > \overline{S_{\rm tot}}$ in the central panel until Thomson scattering takes over, the outward rise of S_{2c} caused by depletion of $n = 2$ when Lyα becomes effectively thin, the collisional domination of the 3c continuum where it emerges, and the steep S_{3c}-at-threshold increase followed by population inversion (lasering, $S_{3c} < 0$) at larger height which results from the Baα losses driving the Rydberg recombination ladder. The source function peak survives edge averaging but is obliterated by Thomson scattering in the total source function.

[3]In Rutten's lecture notes *"Radiative Transfer in Stellar Atmospheres"* the VALIIIC model is elevated to stellar status in order to make it resist all subsequent developments in solar physics – including Avrett's own improvements – and let it remain a star that *perfectly* exemplifies standard modeling assumptions. The Fig. 36 diagrams of Vernazza et al. (1981) supply abundant examination questions to stellar-atmosphere courses teaching static-plane-parallel astrophysics actually obeyed by this star. The true solar atmosphere is dynamic and much more complex, but understanding VALIIIC physics is a test every stellar atmosphere researcher must pass.

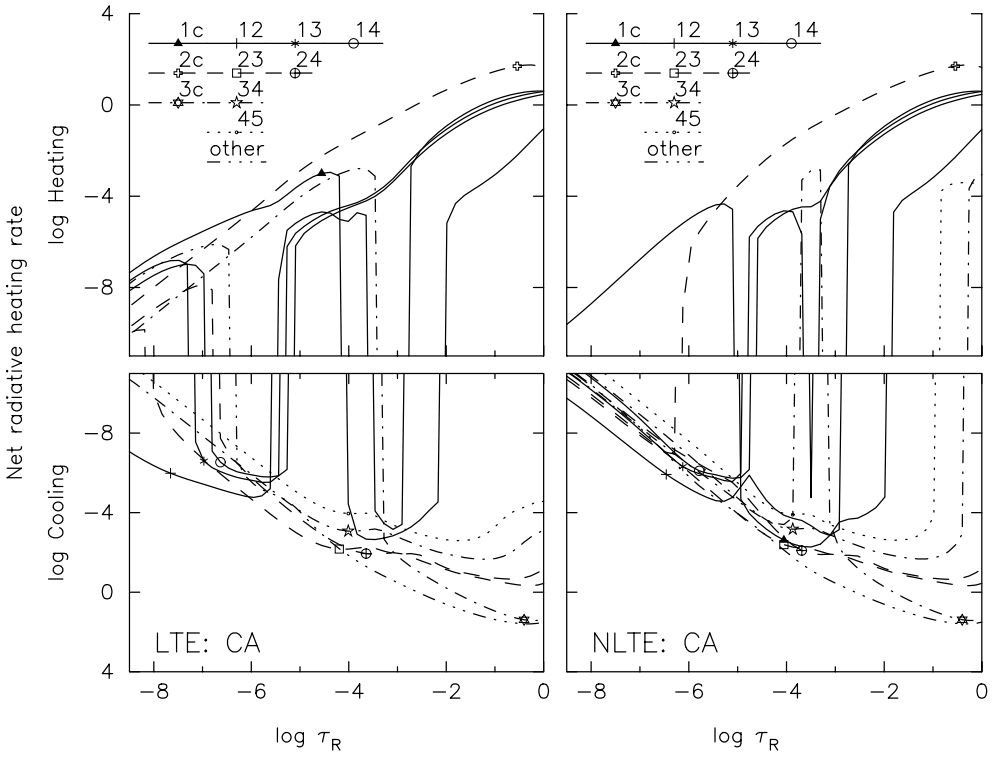

Figure 4. Avrett-style radiative heating contributions $\int \alpha_\nu (J_\nu - S_\nu)\, \mathrm{d}\nu$ of the most important transitions, for the LTE (left) and NLTE (right) complete-atom models respectively. The curve coding differs between lower levels as indicated. The symbols identify $\tau_\nu = 1$ locations per transition with the same coding as in the temperature stratification plots in Fig. 1. The dash-dot-dot-dot curve without symbol near the bottom is the sum of all other contributions (mainly the hydrogen free-free continuum).

Radiation budget graphs. Finally, Fig. 4 shows radiative energy budget diagrams comparable to the VALIIIC graphs in Figs. 48–39 of Vernazza et al. (1981) and giving information similar to the budget tables in Auer & Mihalas (1969a, b), but only for the complete hydrogen model in view of our page limitation. The positive and negative contributions add up to zero because these models obey RE (VALIIIC does not). Note the large ordinate ranges needed to encompass the steep outward decline due to the exponential density decay.

Consider first the LTE budget (lefthand panels). The free-free continuum is the major $J < B$ coolant up to $\log \tau_\mathrm{R} = -4$. The $2c$ Balmer continuum contributes $J > B$ heating throughout the atmosphere, supplying compensation up to $\log \tau_\mathrm{R} \approx -6$ where the Lyman continuum takes over. The optically-thin $2c$ absorption contributes much more heating than the optically-thick line blocking ("backwarming") by the Lyman lines. In contrast, the Paschen $3c$ continuum is a $J < B$ coolant at depth due to the smaller (Rayleigh-Jeans) Planck function sensitivity to the temperature gradient at longer wavelengths, and only flips to

$J > B$ heating at the second dive of the temperature stratification ($\tau_{\rm R} = -3$, see leftmost lower panel of Fig. 1; note that the stratification curvature at this height causes a $J < B$ sign flip for Lyα because its $\mathbf{\Lambda}$ operator covers narrow range).

At the top of the LTE atmosphere Lyα is of course the strongest cooler, compensated by nearly everything else including the Lyman continuum and the higher Lyman lines. Baα is the main cooler around $\log \tau_{\rm R} = -5$. Paα and Brα show similar behavior at lower opacity.

Now turn to the NLTE complete-model budget at right in Fig. 4. The free-free continuum results from LTE processes and maintains its role. The Balmer continuum retains its $J > S$ compensation heating up to the $J = S$ crossing in the center panel of Fig. 3 caused by the Lyα depletion of $n = 2$.

At the top of the atmosphere Lyα remains the major coolant but much less effectively due to its scattering. The Lyman continuum has to provide all the compensation $J > S$ heating, upsetting its two-level resonance-scattering behavior ($S \approx J$) in the lefthand panels of Fig. 3.

Conclusion. We have added various diagnostical displays to the ones in Auer & Mihalas (1969a, b) and also results from a complete hydrogen model. The main coolers are the hydrogen free-free continuum and Lyα even when scattered. Compensation heating occurs in the Balmer and Lyman continua. The photon losses in Baα suck population from the proton reservoir through a collisionally-dominated Rydberg recombination flow and so boost the outward temperature rise.

Assignment. Dear student: explain every curve shown in this contribution.

Acknowledgements. Our debts to Lawrence Auer, Dimitri Mihalas and Eugene Avrett are obvious, large, and shared community-wide. RJR thanks the organizers for an excellent workshop, the Leids Kerkhoven Bosscha Fonds for travel grants, and the Lanz family for hospitality.

References

Auer L. H., Mihalas D., 1969b, ApJ 156, 157

Auer L. H., Mihalas D., 1969c, ApJ 156, 681

Auer L. H., Mihalas D., 1969a, ApJ 156, L151

Bruls J. H. M. J., Rutten R. J., Shchukina N. G., 1992, A&A 265, 237

Carlsson M., Rutten R. J., 1992, A&A 259, L53

Carlsson M., Rutten R. J., Shchukina N. G., 1992, A&A 253, 567

Hubeny I., Lanz T., 1995, ApJ 439, 875

Mihalas D., 1970, 1978, Stellar Atmospheres, W. H. Freeman and Co., San Francisco

Rutten R. J., Carlsson M., 1994, in D. M. Rabin, J. T. Jefferies, C. Lindsey (eds.), Infrared Solar Physics, Proc. Symp. 154 IAU (Tucson), Kluwer, Dordrecht, p. 309

Vernazza J. E., Avrett E. H., Loeser R., 1976, ApJS 30, 1

Vernazza J. E., Avrett E. H., Loeser R., 1981, ApJS 45, 635